An Analysis and Forecasting of Warm-Season Intraseasonal variability

Chung-Hsiung Sui[1,2], Yung-An Lee[1], Yu-Chia Peng[1], Szu-Ying Lee[1]
Institute of Hydrological Sciences, National Central University[1]
Department of Atmospheric Sciences, National Central University[2]

Abstract

Dominant modes of intraseassonal oscillations (ISOs) in May-June and July-August are identified separately by a combined-EOF analysis of vorticity at 850 hPa and outgoing longwave radiation (OLR) within 25°S-25°N and 30°E-160°W for the years 1979-2003. The extracted ISOs account for about 50% and 25% variance of band-pass filtered (15-75 days) and unfiltered OLR, respectively. In May-June, ISOs are identifiable as eastward-moving Madden Julian Oscillations (MJO) with a distinct northward propagation component, which are relatively more active in Indian Ocean than in western Pacific Ocean. A significant phase relation is noted between ISOs and the South China Sea monsoon onset and the subsequent seasonal transition in East Asia. In July-August, ISOs exhibit a stronger propagation signal toward the poles than to the east. The meridional propagating signal is accompanied with strong cyclonic vorticity which is northward in western Pacific and southward in eastern Indian Ocean.

A simple statistical prediction model is developed to explore the predictability of the intraseasonal variability. Preliminary results show the prediction skill significantly better than the persistence, especially at lead time longer than 5 days because prediction skill is quite persistent from 5-day to 25-day but the persistence skill deteriorates rapidly from 5-day to longer lead time. The areas of high prediction skill generally coincide with the centers of action identified by the composite ISOs in May-June and July-August except the area in western Pacific in July-August.

Key word: Intraseasonal Oscillatoins, forecasting

1. Introduction

Tropical intraseasonal variability (ISV) exhibits a strong seasonality. While eastward-moving intraseasonal disturbances found by Madden and Julian (1970) have been widely regarded as fundamental equatorial Kelvin-Rossby waves termed Madden-Julian oscillations (MJO), instraseasonal disturbances in the warm season exhibit a distinct pole-ward propagation component in Indian Ocean in May and June, and in western Pacific in late warm season (e.g. August-October by Kemball-Cook and Wang 2001). Such seasonal dependent feature is in phase with the different onset times of the East Asian summer monsoon (EASM) and Western North Pacific summer monsoon (WNPSM) (see Wang and Lin 2002). Observed features and relevant mechanisms are discussed in Wang & Xie (1996) and Jiang et al. (2003) who demonstrated that the vertical shear of zonal monsoon flow provides a favorable condition conducive to the northward propagation of the eastward-moving ISOs. In addition, air-sea interaction and the moisture gradient in the planetary boundary layer over the warm water in Indian Ocean and west Pacific Ocean may also be important.

The warm-season intraseasonal disturbances in the Asian monsoon region are accompanied by high frequency wave disturbances including synoptic-scale disturbances and tropical cyclones which tend to move northwestward (Lau and Lau 1990, 1992). These various disturbances of the multiscale disturbances are mutually correlated, making scale separation a challenging yet important issue for the study of interest.

The goals of the present study are 1) to identify the dominant mode of the intraseasonal variability, hereafter referred to as intraseasonal oscillation (ISO), in May-June (EASM period) and July-August (WNPSM period) within the tropical Indo-Pacific region, 2) to study causal relations between ISOs, monsoon, Antarctic annular oscillations (AAO), high-frequency disturbances, 3) to examine the interannual variability of ISOs, 4) to explore the predictability of ISOs by statistical-dynamic models. Results related to the first and fourth goals are reported here.

2. Dominant modes of ISV

This study employs the outgoing longwave radiation (OLR) and wind at 200 and 850 hPa from the NCEP reanalysis for 1979-2003. The data are processed into two sets: a band-pass filtered set and an anomalous set. The band-pass filtered set of data is obtained by 1) applying the Empirical Normal Mode Analysis (ENMA) method (Lee 2005) to each variable for each one-year, $Xij(r,t)$ (i denotes each of the five daily variables OLR, u_{200}, v_{850}, u_{850}, v_{850}; j denotes each of the 25 years), to decompose $Xij(r,t)$ into empirical normal modes (ENM)

$$X_{ij}(r,t) = \sum_k e^{i\omega_k t} ENM_k(r),\ \omega_k = 2\pi k/365,\ k = 1-182,$$

2) retaining the annual sub-harmonics wave number 5-37 (10-75 day) of each variable in each year, to reconstruct

the band-pass filtered data, $<X_i>$. The anomalous data, X_i', is obtained by removing the first three harmonics of climatological annual cycle of daily data, and removing the synoptic scale variability by 3-day running average three times.

Then a combined EOF analysis and SVD analysis are applied to various combination of band-passed filtered data within the domain (25°S-25°N, 30°E-160°W) to extract the dominant ISOs. The percentages of variance accounted for by the first four PCs of OLR by the various analyses are listed in Table 1 and 2 for the period May-June and July-August, respectively. It is obvious that the combined EOF analysis and SVD analysis of OLR and 850 hPa vorticity extract the highest variance. The reconstructed intraseasonal variability using the first two modes account for about 50% and 25% variance of band-pass filtered and unfiltered data, respectively.

Table 1 Per cent of σ^2_{OLR} (May-June 1979-2003)

Analysis method \ mode		1st	2nd	3rd	4th
(OLR) EOF		9.5	7.0	4.9	4.1
(OLR, $\mathbf{V}_{200}$, $\mathbf{V}_{850}$)	C-EOF	8.6	6.4	4.5	3.7
(OLR, $\mathbf{V}_{200}$–$\mathbf{V}_{850}$)	C-EOF	8.9	6.6	4.6	3.7
(OLR, $\mathbf{V}_{200}$+$\mathbf{V}_{850}$)	C-EOF	8.3	6.2	4.5	3.8
(OLR, $vort_{200}$)	C-EOF	10.2	6.3	4.5	3.6
(OLR, $vort_{850}$)	C-EOF	10.0	6.4	4.5	3.6
(OLR, $vort_{200}$)	SVD	20.2	15.9	12.4	8.5
(OLR, $vort_{850}$)	SVD	32.3	15.8	8.1	5.8

Table 2 Per cent of σ^2_{OLR} (July-August 1979-2003)

Analysis method \ mode		1st	2nd	3rd	4th
(OLR, $vort_{200}$)	C-EOF	8.6	6.0	5.5	4.1
(OLR, $vort_{850}$)	C-EOF	8.5	6.5	5.5	4.2
(OLR, $vort_{200}$)	SVD	17.1	10.3	9.1	7.9
(OLR, $vort_{850}$)	SVD	31.9	15.7	9.8	6.9

The PCs of the first two modes can be used to define the phase and amplitude of ISOs:

$\theta = tan^{-1}(PC1/PC2)$, $Amp = (PC1^2+PC2^2)$.

The set values of (PC1, PC2) or (θ, Amp) for ISOs in May-June and July-August is called MJ indices and JA indices. Based on the value of θ obtained by the C-EOF analysis of vorticity at 850 hPa and OLR, eight phases are defined for each cycle of ISOs and the anomalous data are used to form a composite cycle separately for May-June and July-August (Fig. 1 and 2). Figure 1 and 2 also include composite MJOs based on the indices following Wheeler and Hendon (2004), referred to as WH04. Note that the indices calculated in WH04 are called RMM indices.

Although the phases of ISOs based on MJ and JA indices and that based on RMM indices are derived differently, they are quite similar in May-June and the composite ISO and MJO have common dominant features, in terms of phase, propagation, and spatial structure. Figure 1 also show that ISOs are more active in Indian ocean than in W. Pacific. Table 3 summarizes coincidence of the onset time of South China Sea monsoon and the ISO phase transition from 4 to 5 (see Fig. 1). The significant relation suggests that the ISOs often facilitate the seasonal transition and the subsequent Meiyu front development in SE Asia.

Table 3 Coincidence of the onset time of SCS monsoon and the ISO phase transition from 4 to 5

The onset of the SCS Monsoon	Year
in-phase with both indices	1979, 1980, 1982, 1983, 1985, 1987, 1988, 1991, 1992, 1994, 1995, 1997, 1998, 1999
in phase with MJ in phase with RMM	1981, 1986, 1996 1989, 1993
out of phase with both indices	1984, 1990, 2000, 2001

ISOs in July-August are closely in phase with MJOs but have stronger meridional propagating than eastward propagating signals. The meridional propagating signal is accompanied with strong cyclonic vorticity which is northward in western Pacific and southward in eastern Indian Ocean. The disturbances are more active in W. Pacific than in Indian ocean

3. Statistical Prediction Model

A simple AR1 model is developed evaluate the predictability of intraseasonal variability, i.e.,

$$\mathbf{Y}(t+\tau) = \mathbf{A}\,\mathbf{Y}(t)$$

where $\mathbf{Y}(x, t)$ denotes the predictor which is a function of $x \in (1, \ldots m)$ and time $t \in (1, \ldots n+1)$, and $\mathbf{Y}(x, t+\tau)$ denotes the predictand that lags $\mathbf{Y}(x, t)$ by τ period, and $\mathbf{A}$ is the linear propagator. In this study, x denotes significant empirical normal modes. For multivariates, m = number of variables × number of significant modes of each variable. $\mathbf{A}$ can be solved by the following steps:

1) $\mathbf{Y}(t)$ and $\mathbf{Y}(t+\tau)$ are reconstructed by EOF filtering to retain significant modes;

2) to solve $\mathbf{A}$ by Singular Value Decomposition of $\mathbf{Y}$, $\mathbf{Y}(t)=\mathrm{E}\Lambda\mathrm{F}^{\mathrm{T}}$, so $\mathbf{A} = \mathbf{Y}(t+\tau)\mathbf{Y}^{-1}(t) = \mathbf{Y}(t+\tau)\mathrm{F}\Lambda^{-1}\mathrm{E}^{\mathrm{T}}$;

In this study, EOF analysis is applied to the data to retain dominant empirical orthogonal modes in estimateing $\mathbf{A}$ and to forecast. while ENMA (Lee 2005) uses unfiltered data to estimate $\mathbf{A}$ and then uses only normal modes of peak spectra to predict. As a result, AR1 is optimal for short leads forecast, while ENMA is optimal for long leads forecast.

To test the skill of the AR1 model on predicting intraseasonal variability, we solve $\mathbf{A}$ based on pentad OLR within a window of two- to four-months period centered at t and $t+\tau$. Here τ is 5, 10, 15, 20, or 25 days, and t is the prediction time within the warm season (May to August). A systematic check reveals that prediction is insensitive to the number of retained EOF modes (significant skill already obtained by 2 PCA modes), nor to the window length of predictor and predictand

To verify the prediction skill, we select each warm season of the 25 years as prediction target and the rest of 24 warm seasons to estimate $\mathbf{A}$. The temporal correlation between predicted OLR of 5, 10, 15, 20, 25 day lead time

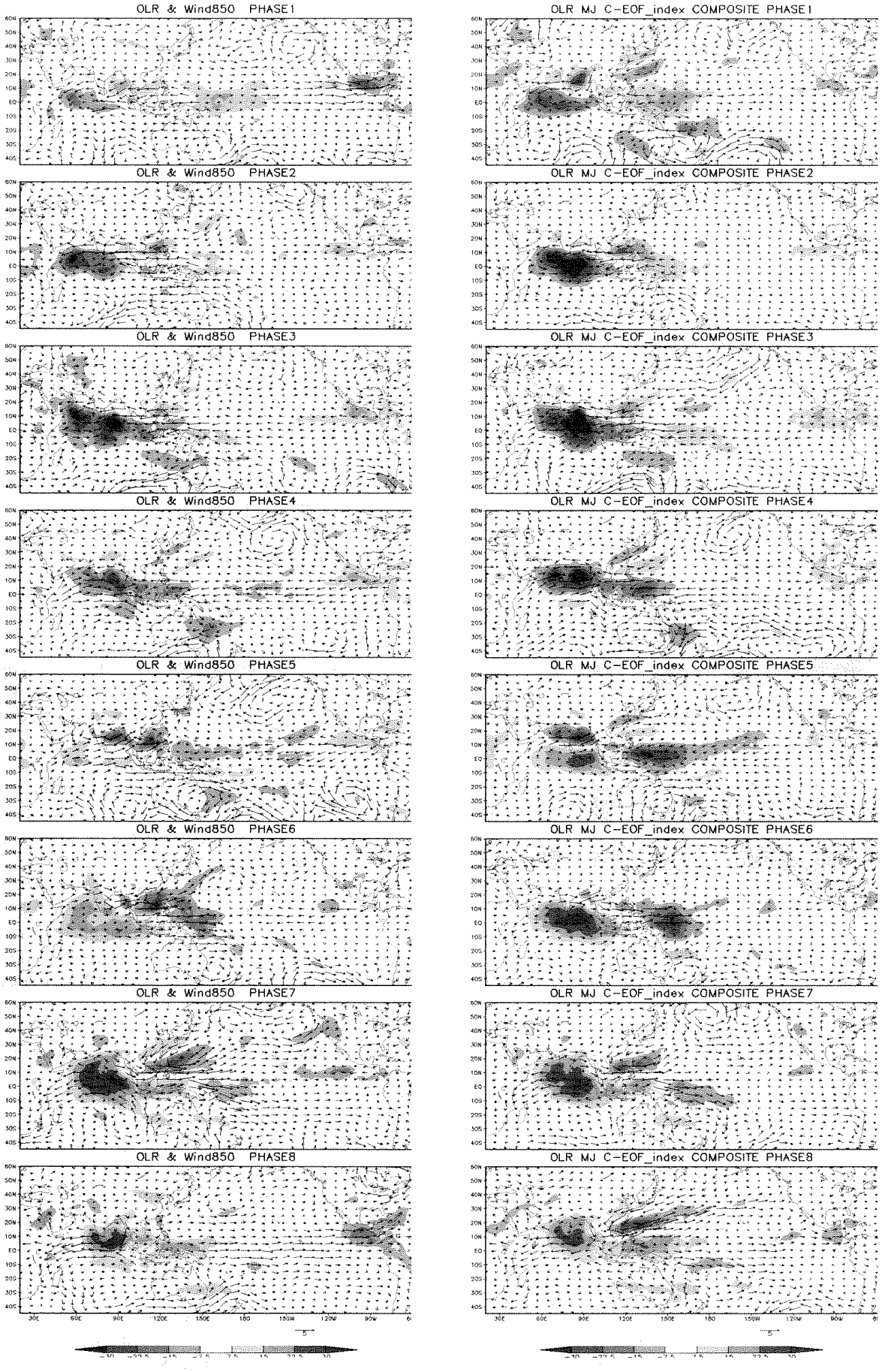

Fig. 1 Composite OLRA and 850-hPa wind vector anomalies for May-June based on RMM indices (left) and MJ indices . The magnitude of the largest vector is shown on the bottom right.

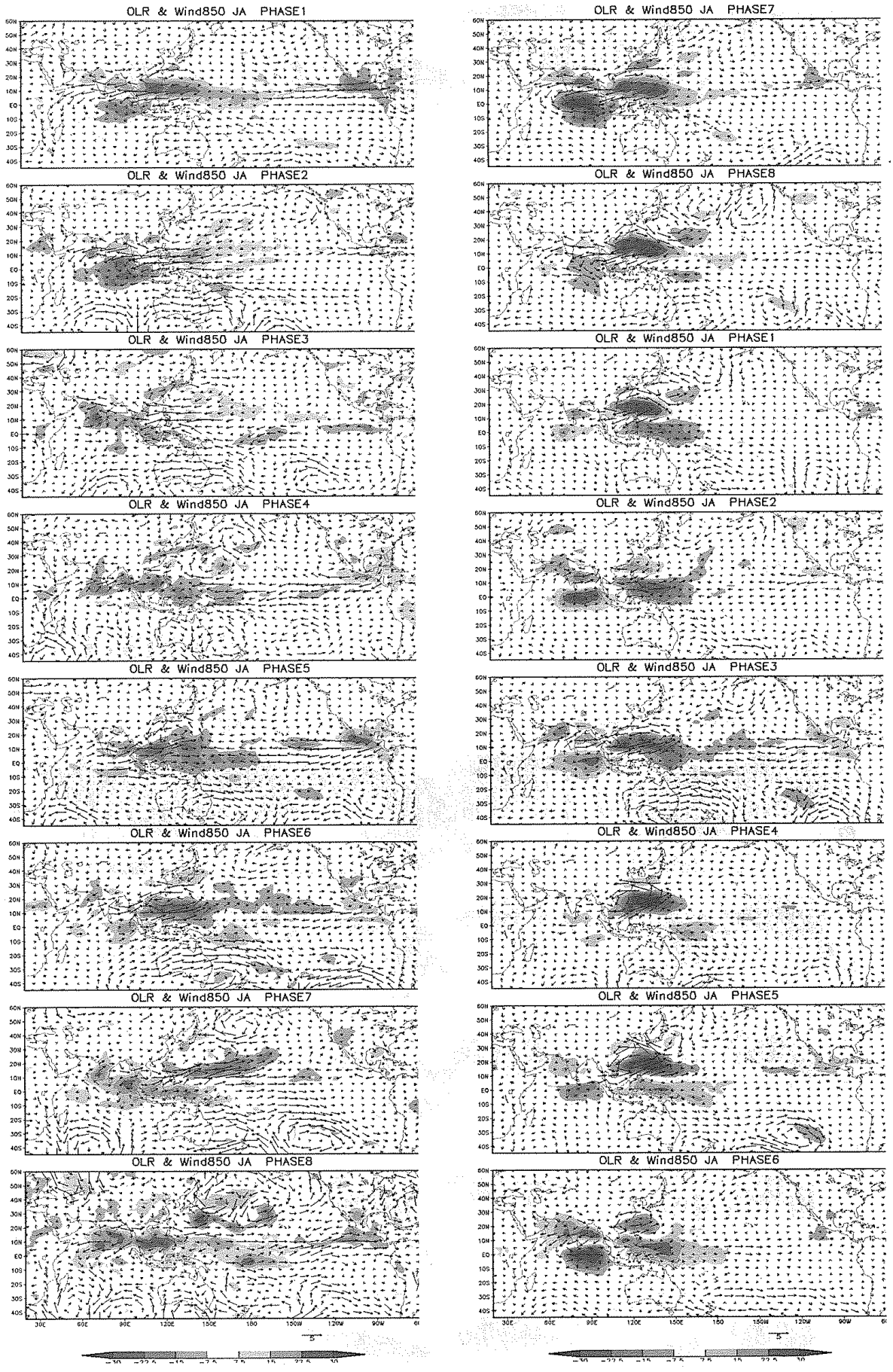

Fig. 2 Composite OLRA and 850-hPa wind vector anomalies for July-August based on RMM indices (left) and JA indices . The magnitude of the largest vector is shown on the bottom right.

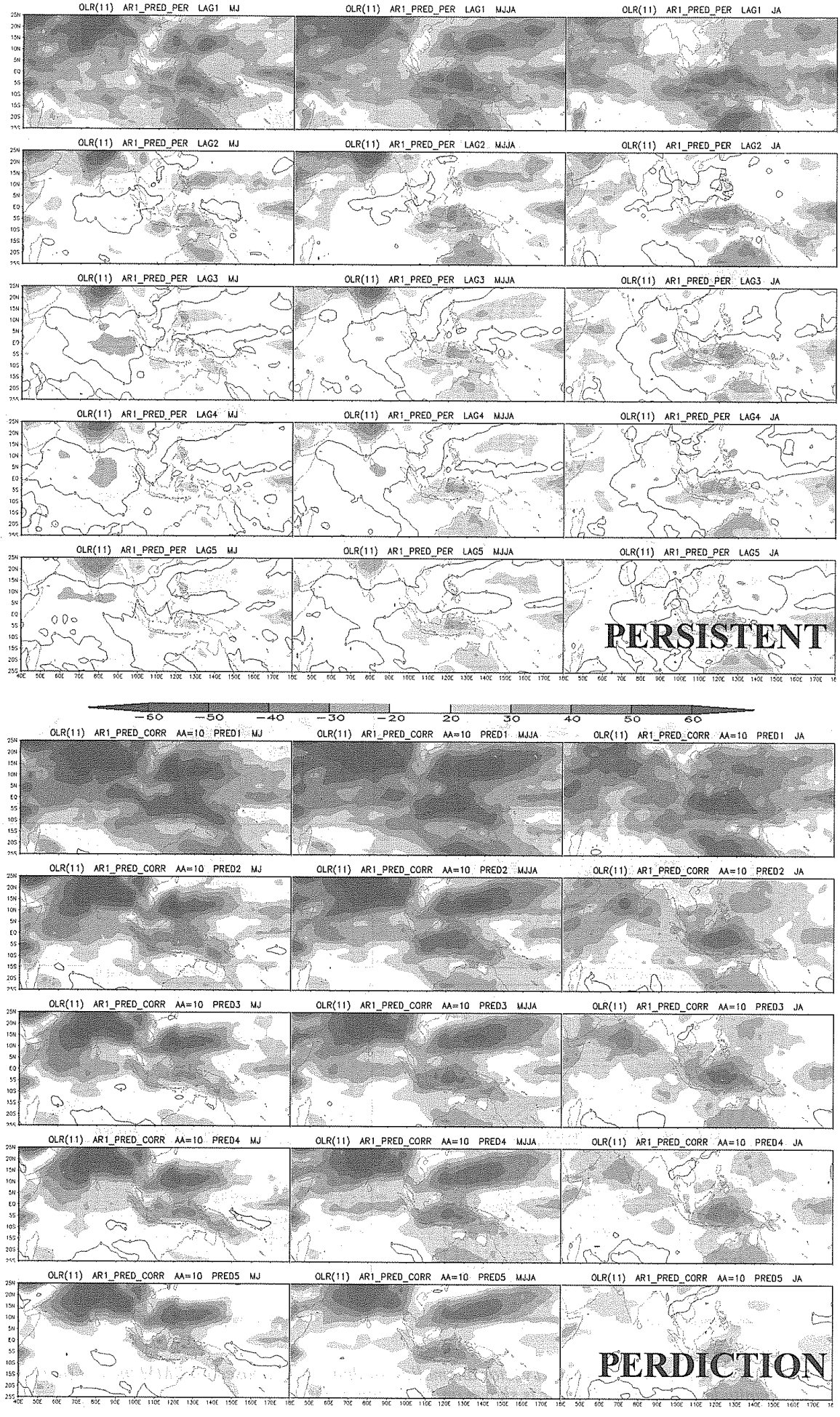
OLR(11) AR1_PRED_PER LAG1 MJ
OLR(11) AR1_PRED_PER LAG1 MJJA
OLR(11) AR1_PRED_PER LAG1 JA
OLR(11) AR1_PRED_PER LAG2 MJ
OLR(11) AR1_PRED_PER LAG2 MJJA
OLR(11) AR1_PRED_PER LAG2 JA
OLR(11) AR1_PRED_PER LAG3 MJ
OLR(11) AR1_PRED_PER LAG3 MJJA
OLR(11) AR1_PRED_PER LAG3 JA
OLR(11) AR1_PRED_PER LAG4 MJ
OLR(11) AR1_PRED_PER LAG4 MJJA
OLR(11) AR1_PRED_PER LAG4 JA
OLR(11) AR1_PRED_PER LAG5 MJ
OLR(11) AR1_PRED_PER LAG5 MJJA
OLR(11) AR1_PRED_PER LAG5 JA
PERSISTENT
−60 −50 −40 −30 −20 20 30 40 50 60
OLR(11) AR1_PRED_CORR AA=10 PRED1 MJ
OLR(11) AR1_PRED_CORR AA=10 PRED1 MJJA
OLR(11) AR1_PRED_CORR AA=10 PRED1 JA
OLR(11) AR1_PRED_CORR AA=10 PRED2 MJ
OLR(11) AR1_PRED_CORR AA=10 PRED2 MJJA
OLR(11) AR1_PRED_CORR AA=10 PRED2 JA
OLR(11) AR1_PRED_CORR AA=10 PRED3 MJ
OLR(11) AR1_PRED_CORR AA=10 PRED3 MJJA
OLR(11) AR1_PRED_CORR AA=10 PRED3 JA
OLR(11) AR1_PRED_CORR AA=10 PRED4 MJ
OLR(11) AR1_PRED_CORR AA=10 PRED4 MJJA
OLR(11) AR1_PRED_CORR AA=10 PRED4 JA
OLR(11) AR1_PRED_CORR AA=10 PRED5 MJ
OLR(11) AR1_PRED_CORR AA=10 PRED5 MJJA
OLR(11) AR1_PRED_CORR AA=10 PRED5 JA
PERDICTION

Fig. 3 (Upper 15 panels) Skill of persistence calculated by lagged temporal correlation of observed OLR for May-June (left), May-August (middle), July-August (right), 1979-2003. The lag time 5, 10, 15, 20, 25 days (1st to 5th row). (Lower 15 panels) Similar to the upper 15 panels except for the temporal correlation between observed and predicted OLR of lead time 5, 10, 15, 20, 25 days.

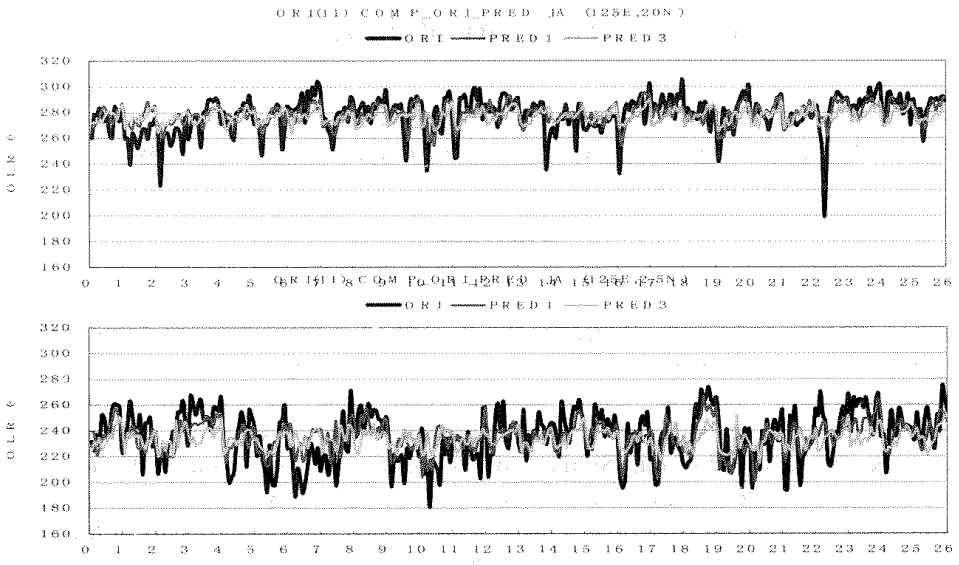

Fig. 4 Time series of observed OLR against 5-day and 15-day predicted OLR at selected points A (125^{0}E , 20^{0}S) (upper) and B(120^{0}E , 2.5^{0}S) (lower) where persistent skills are high.

and the corresponding observed OLR at each grid within the domain of interest is shown in Fig. 3. Also shown is the corresponding skill of persistence. The skill of the simple AR1 is significantly better than the persistence, especially at lead time longer than 5 days because prediction skill is quite persistent from 5-day to 25-day but the persistence skill deteriorates rapidly from 5-day to longer lead time. The areas of high prediction skill generally coincide with the centers of action identified by the composite ISOs in May-June and July- August (Fig. 1 and 2) except the area in western Pacific in July-August.

To further check the temporal variability of the predicted OLR, the time series of 5-day and 15-day prediected ORL are plotted in Fig. 4 against the observed OLR at two selected points (120^{0}E , 2.5^{0}S) and (120^{0}E , 20^{0}S) where the persistent skills are high. The predicted convective activities as shown by negative OLRs are in good agreement with those of the observed values.

References

Jiang, X., T. Li, and B. Wang, 2003: Structures and Mechanisms of the Northward Propagating Boreal Summer Intraseasonal Oscillation. *J. Climate*, **17**, 1022–1039.

Kemball-Cook, S. R., and B. Wang, 2001: Equatorial waves and air–sea interaction in the boreal summer intraseasonal oscillation. *J. Climate*, **14**, 2923–2942.

Lau, K.-H., and N.-C. Lau, 1990: Observed structure and propagation characteristics of tropical summertime synoptic scale disturbances. *Mon. Wea. Rev.*, **118**, 1888–1913.

Lau, K.-H., and N.-C. Lau, 1992: The energetics and propagation dynamics of tropical summertime synoptic-scale disturbances. *Mon. Wea. Rev.*, **120**, 2523–2539.

Lee, Yung-An, 2005 : Empirical Normal Mode Analysis *J. Climate* (in revision).

Wang, B, and X. Xie, 1996: Low-Frequency Equatorial Waves in Vertically Sheared Zonal Flow. Part I: Stable Waves. *J. Atmos. Sci.*, **53**, 449–467.

Wang, B, and LinHo, 2002: Rainy Season of the Asian–Pacific Summer Monsoon. *J. Climate*, **15**, 386–398.

Wheeler, M.C., H.H. Hendon, 2004: An All-season Real-time Multivariate MJO Index: Development of an Index for Monitoring and Prediction. *Mon. Wea. Rev.* **132**, No. 8, 1917–193